Trajectory tracking control of self-driving farming vehicle based on nonsingular fast terminal sliding mode and finite time disturbance observer

Zhanmeng Lin, Xiaohong Jiao, Ting Zhang

Institute of Electrical Engineering, Yanshan University, Qinhuangdao, 066004 China (e-mail: jiaoxh@ysu.edu.cn)

Abstract: Aiming at parameter perturbations and external disturbances, a robust finite-time trajectory tracking control strategy is proposed to enhance self-driving farming vehicles' system trajectory tracking performances. A kind of finite time disturbance observer (FDO) is designed to enhance the system's robustness and minimize the chattering effects. The nonsingular fast terminal sliding mode (NFTSM) surface is constructed to improve the system's response speed and anti-disturbance behavior. The Lyapunov stability approach proves the finite-time stability of the closed-loop control system. The effectiveness and advantages of the designed control strategy are illustrated by a simulation scenario and by comparing with some existing methods under several simulation conditions in the CarSim-Simulink environment.

Keywords: self-driving farming vehicle, trajectory tracking, nonsingular fast terminal sliding mode (NFTSM), finite time disturbance observer (FDO), finite-time stability

1. INTRODUCTION

The automatic driving of agricultural machinery has become one of the primary and effective technologies to promote the development of modern agriculture to save labor and reduce labor intensity (Bochtis et al, 2014). The self-driving agricultural machinery has also essentially facilitated the transition from traditional agriculture to precision agriculture based on modern advanced computing, actuating, and sensing technologies (Tzounis et al, 2017). Various farming operations have used automatic driving agricultural machineries, such as weeding, agricultural chemical spraying, crop monitoring, and harvesting. It has shown the advantages of high operating efficiency and low operating cost (Li et al, 2019). However, it has become a hot topic how to accurately track the predetermined trajectory of the automatic driving agricultural machinery through modern control technology in developing automated driving technology (Roshanianfard et al, 2020). In addition, the finite-time control strategy has been applied to increasingly complex agricultural operations gradually because of its ability to achieve rapid convergence of the controlled system and the fast and accurate trajectory tracking control of the autonomous agricultural machinery.

Due to the agricultural operation environment's complexity, many disturbance problems exist in the trajectory tracking process of the self-driving farming vehicle (SDFV) (Watanabe et al, 2021). The disturbance problems will directly affect the accuracy of trajectory tracking of the controlled system, thus affecting agricultural production. Therefore, there are many control methods proposed to solve these problems, such as active disturbance rejection control (ADRC) (Xia et al, 2016), sliding mode control (SMC) (Sun et al, 2019; Wu et al, 2019). As a control theory developed based on the PID control algorithm, the ADRC integrates the advantages of simple design and high tracking accuracy and has a solid anti-disturbance ability. A linear ADRC strategy is designed in (Chao et al, 2018) for a robotic vehicle to suppress the disturbance effects caused by the lateral and longitudinal slips during driving. Although the ADRC has the advantage of solid robustness, selecting its control parameters still depends on the experience and trial. (Lin et al, 2019) proposes a particle swarm optimization algorithm to solve the problem of complex parameter selection in ADRC and shows that the controlled system has higher tracking accuracy in linear tracking by the simulation results. However, the tracking accuracy and response speed of the controlled system need improving in the process of curve tracking. The SMC has been widely used in trajectory tracking control because of its robustness. The trajectory tracking SMC strategy is proposed in (Soudbakhsh et al, 2011) to resist the effects of disturbances and improve the trajectory tracking accuracy of the controlled system. (Jiang et al, 2015) proposes a robust trajectory tracking control scheme for agricultural vehicles based on finite-time control and sliding mode observer. The dynamic tracking performance is improved, but only for the straight-line tracking process. However, curve trajectory tracking is inevitable in the actual agricultural operation process. (Wang et al, 2012; Lv et al,, 2017) propose the NFTSM control for surface ships to solve the disturbance problems in the trajectory tracking process. The NFTSM has strong robustness to disturbance and improves the fast response performance of the controlled system. In addition, chattering problems in the SMC, as an

⋆ This work was supported by the National Natural Science Foundation of China (Grant No.61973265).

inevitable defect, have been extensively studied (Matveev et al, 2013). The SMC based on the extended state observer (ESO) has been widely applied to the actual trajectory tracking process to suppress the adverse effects caused by disturbance and uncertainty. Meanwhile, the ESO-based SMC is also beneficial in stopping the effects of chattering. For example, there is the ESO-based integral SMC for the underwater robot (Cui et al, 2017) and the terminal SMC based on the ESO for the automotive transmissions clutch control process (Li et al, 2016).

Motivated by the analysis above, this paper investigates a robust finite-time trajectory tracking control strategy based on the NFTSMC and the FDO for the SDFV. The main contributions are summarized as follows: (i) A FDO (seen as Eq.(5)) is designed to enhance the system's robustness to disturbance and minimize the chattering effects. (ii) A NFTSM switching function (seen as Eq.(9)) is constructed to improve the response speed and anti-disturbance behavior of the controlled system in the presence of parameter perturbations and external disturbances. (iii) The effectiveness and advantages of the designed FDO-based NFTSMC strategy (NFTSM-FDO) (seen in Eq.(13) with Eq.(5) and Eq.(9)) are illustrated by comparing it with the controller presenting the same control structure (Wu et al, 2019) and the controller based on ADRC under the CarSim-Simulink environment.

This paper is organized as follows. Section 2 describes and models the farming vehicle operation process. Section 3 designs a nonsingular fast terminal sliding mode controller with a finite time disturbance observer and proves the stability of the controlled system by the Lyapunov stability approach. Section 4 presents simulation results. This paper is concluded in section 5.

The following abbreviations are used in this manuscript:

ADRC	Active disturbance rejection control
CG	Center of gravity
DOF	Degree of freedom
ESO	Extended state observer
FDO	Finite time disturbance observer
NFTSM	Nonsingular fast terminal sliding mode
NFTSMC	NFTSM control
PID	Proportion Integration Differentiation
SDFV	Self-driving farming vehicle
SISO	Single-input-single-output
SMC	Sliding mode control

2. FARMING VEHICLE OPERATION PROCESS-DESCRIPTION AND MODELING

2.1 Autonomous farming vehicle operation process

Fig. 1 shows the typical operating trajectory of the SDFV. (x_{ref}, y_{ref}, φ_{ref}) represents the vehicle's reference position and yaw angle information in the Earth coordinate system, and (x, y, φ) represents the actual position and yaw angle value of the SDFV in the field. This paper assumes that the SDFV turns through the front wheels, and the rear wheels provide the driving force. Moreover, when the research focuses on lateral motion control, some factors, such as the dynamic process of the actuator motor, can be ignored. At this time, the actual control input is only proportional to the front wheel steering angle. Thus, the front wheel steering angle δ_f is regarded as the control input of the lateral movement, as in (Wu et al, 2019). The operation requires the SDFV to travel in one row, turn at the end, and enter the next row. Throughout the process, straight-line trajectory tracking accounts for a large proportion, and its tracking accuracy is relatively easy to achieve. At the same time, the accuracy of curve trajectory tracking is also essential. It can ensure that the SDFV smoothly and accurately enters into the following line of operation process (Lipinski et al, 2016).

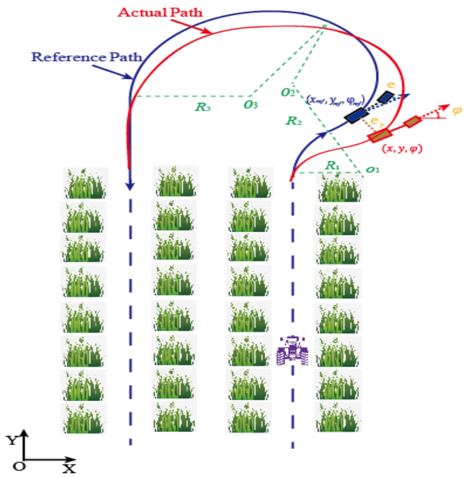

Fig. 1. Operating trajectory of SDFV.

High precision tracking is accessible in the SDFV straight-line trajectory tracking, so its tracking error is tiny. However, a large tracking error might appear when the SDFV is affected by the disturbance or the curve tracking process. In this case, the front wheel steering angle of the SDFV needs real-time control so that the vehicle's yaw angle φ is consistent with the reference yaw angle φ_{ref} to make the yaw angle tracking error e and the lateral direction tracking error e_y small. Therefore, the purpose of the control is to design a controller so that the yaw angle tracking error and lateral tracking error converge to zero as quickly as possible.

2.2 System model description

The 'bicycle' model (2-DOF dynamics model) shown in Fig. 2 is adopted for the description of the SDFV, which is adapted from (Wu et al, 2019). The coordinate based on the earth is XOY. The coordinate xoy represents the coordinate system of the SDFV. The vehicle kinematics is modeled with the center of gravity (CG) as the reference point. Make the following assumptions:

(i) The trajectory tracking requirements can be achieved by controlling the front wheel steering angle of the autonomous ground vehicle to accurately control the lateral movement of the vehicle (Wu et al, 2019).

(ii) The SDFV is driven on the field with a constant longitudinal velocity as generally required in the automatic guidance of agricultural vehicles.

(iii) The slip angles of the SDFV are generally relatively small in the process of low-speed driving.

(iv) For the SDFV model, the parameters C_r, C_f (the steering stiffness of the front and rear wheels), and I_z (the yaw moment of inertia) are easy to change under the influence of the environment and difficult to obtain directly. The variations of these parameters have significant impacts on trajectory tracking control, which can not be ignored.

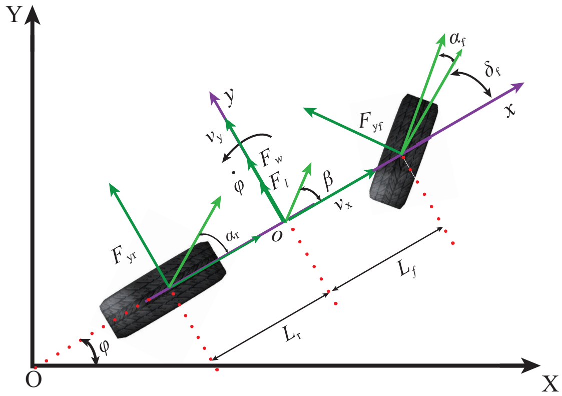

Fig. 2. 'Bicycle' model adapted from (Wu et al, 2019).

The variable descriptions in Fig. 2 are shown in Table 1.

Table 1. Variable descriptions shown in Fig. 2.

Variable	Description
φ	Yaw angle
$\dot{\varphi}$	Yaw rate
v_y	Lateral velocity
v_x	Longitudinal velocity
δ_f	Front wheel steering angle
F_{yf}	Lateral force at front axle
F_{yr}	Lateral force at rear axle
α_f	Sideslip angle at front axle
α_r	Sideslip angle at rear axle
L_f	Distance from the CG to front axle
L_r	Distance from the CG to rear axle
β	Slip angle at the CG
o	The CG of the vehicle

Accordingly, the 2-DOF vehicle plane motion model can be expressed as follows:

$$\begin{cases} \dot{X} = v_x \cos\varphi - v_y \sin\varphi \\ \dot{Y} = v_x \sin\varphi + v_y \cos\varphi \\ m(\dot{v}_y + v_x\omega) = F_{yf} + F_{yr} + F_l \\ \dot{\varphi} = \omega \\ I_z\dot{\omega} = L_f F_{yf} - L_r F_{yr} + M_z \end{cases} \tag{1}$$

where X and Y are the longitudinal and lateral displacements of the vehicle in the XOY coordinate, respectively. m is the vehicle mass. F_l is the unknown lateral disturbance force. I_z is the yaw moment of inertia. M_z is the uncertain yaw torque.

The linear functions can approximately describe the nonlinear tire forces in this driving environment. Moreover, the tire forces are proportional to the slip angles, as shown below (Piyabongkarn et al, 2009; Geng et al, 2009):

$$F_{yf} = -C_f\alpha_f, \quad F_{yr} = -C_r\alpha_r \tag{2}$$

where C_f and C_r are steering stiffness of the front and rear wheels, respectively.

By the small-angle approximation, the expressions of the $\alpha_f, \alpha_r, \beta$ are given as (Wu et al, 2019)

$$\begin{cases} \alpha_f = \beta + \omega L_f/v_x - \delta_f \\ \alpha_r = \beta - \omega L_r/v_x \\ \beta = \arctan(v_y/v_x) \approx v_y/v_x \end{cases} \tag{3}$$

Note that (1) is a typical underactuated system, and the yaw angle φ tracking can be easily realized by controlling δ_f. The dimension reduction of the system can effectively reduce the complexity of the control. If it is possible to construct the desired yaw angle φ_{ref} satisfies that when the vehicle's yaw angle satisfies $\varphi \to \varphi_{ref}$ the displacement deviation can converge to 0. Then, the trajectory tracking process of the SDFV can be achieved by tracking the desired yaw angle and greatly reducing the complexity of the controlled system. As a consequence, substituting (2) and (3) into the yaw motion equation of (1), a control design-oriented dynamic system is obtained as:

$$\begin{cases} \dot{\varphi} = \omega \\ \dot{\omega} = \dfrac{(C_{r0}L_r - C_{f0}L_f)\beta}{I_{z0}} - \dfrac{C_{r0}{L_r}^2 + C_{f0}L_f^2}{I_{z0}v_x}\omega \\ \quad + {I_{z0}}^{-1}C_{f0}L_f u + d_1 \end{cases} \tag{4}$$

where $u = \delta_f$ is the control input. The yaw angle φ is the system output. C_{f0}, C_{r0} and I_{z0} are the nominal parameters. d_1 represents the lumped disturbance consisting of vehicle parameter uncertainties and unknown disturbance from M_z/I_z.

Therefore, the controller design uses the second-order model (4). The control mission is to control vehicle steering through the design of the front wheel angle, reduce the deviation of the heading angle and lateral distance of the farming vehicle when driving along the planned trajectory, and realize the accurate tracking of the vehicle's trajectory.

3. NFTSM-FDO CONTROL STRATEGY DESIGN

This section designs a NFTSM-FDO control strategy for the SDFV trajectory tracking control system. The FDO is for estimating and compensating lumped disturbance to guarantee the robustness of the controlled system. The adopted NFTSM switching function improves the system's response speed and anti-disturbance.

Fig. 3 shows the configuration of the trajectory tracking control system. It should be mentioned that three derivative blocks (d/dt) in Fig. 3 are implemented by the approximate differentiator $\kappa s/(\tau s+1)$, where s is the Laplace variable, κ is the gain filter (chosen as 0.001), and τ is a small number (chosen as 0.01) (refer to (Jiao et al, 2014)).

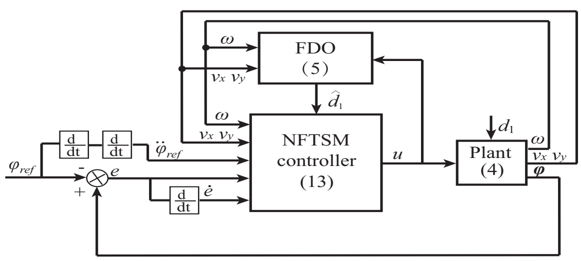

Fig. 3. Configuration of trajectory tracking control system.

3.1 The FDO design

In this subsection, an FDO is developed based on the idea of (Shtessel et al, 2007) to estimate the lumped disturbance. When φ and ω are measurable for the system (4), and there is a Lipschitz constant $L_1 > 0$ for the continuous lumped disturbance $d_1(t)$, the FDO estimating the total disturbances is designed as follows.

$$\begin{cases} \dot{\widehat{\omega}}=I_{z0}{}^{-1}(C_{r0}L_r-C_{f0}L_f)\beta+I_{z0}{}^{-1}C_{f0}L_f u \\ \qquad -(I_{z0}v_x)^{-1}(C_{r0}L_r^2+C_{f0}L_f^2)\omega+m_0 \\ \dot{\widehat{d}}_1=-\lambda_2 L_1\mathrm{sign}(\widehat{d}_1-m_0) \end{cases} \tag{5}$$

where C_{r0}, C_{f0} and I_{z0} are nominal parameters. $m_0 = -\lambda_1 L_1^{\frac{1}{2}}|\widehat{\omega}-\omega|^{\frac{1}{2}}\mathrm{sign}(\widehat{\omega}-\omega)+\widehat{d}_1$, $\widehat{\omega}$ is the estimate of ω, $\widehat{d}_1$ is the estimate of d_1. $\mathrm{sign}(\cdot)$ is the standard sign function. λ_1 and λ_2 are positive adjustable parameters.

The errors between the estimations of the yaw rate and lumped disturbance and their actual values are defined as ε_1 and ε_2, respectively.

$$\varepsilon_1 = \widehat{\omega}-\omega, \quad \varepsilon_2 = \widehat{d}_1 - d_1$$

The dynamic of the observation error can be obtained using equation (6):

$$\begin{cases} \dot{\varepsilon}_1 = m_0 - d_1 \\ \qquad = -\lambda_1 L_1^{\frac{1}{2}}|\widehat{\omega}-\omega|^{\frac{1}{2}}\mathrm{sign}(\widehat{\omega}-\omega)+\widehat{d}_1-d_1 \\ \qquad = -\lambda_1 L_1^{\frac{1}{2}}|\varepsilon_1|^{\frac{1}{2}}\mathrm{sign}(\varepsilon_1)+\varepsilon_2 \\ \dot{\varepsilon}_2 = -\lambda_2 L_1\mathrm{sign}(\widehat{d}_1-m_0)-\dot{d}_1 \\ \qquad \in -\lambda_2 L_1\mathrm{sign}(\varepsilon_2-\dot{\varepsilon}_1)+[-L_1, L_1] \end{cases} \tag{6}$$

The finite-time convergence of the observation errors $\varepsilon_1, \varepsilon_2$ can be proofed by applying the following lemma that is adapted from Lemma 2 in (Shtessel et al, 2007).

Lemma 1. (Shtessel et al, 2007) Consider the SISO system

$$\dot{\sigma} = g(t) + u, \quad \sigma \in R \tag{7}$$

where u is control input, σ is the measured output of the system, and $g(t)$ is an uncertain function whose Lipschitz constant is L. Let ε be the Lebesgue-measurable noise bounded of $\sigma(t)$. Then, the system:

$$\begin{cases} \dot{z}_0 = -\chi_0 L^{\frac{1}{2}}|z_0-\sigma|^{\frac{1}{2}}\mathrm{sign}(z_0-\sigma)+z_1+u \\ \dot{z}_1 = -\chi_1 L\mathrm{sign}(z_0-\sigma) \end{cases}$$

is a nonlinear observer for $g(t)$, and $z_0(t)$ and $z_1(t)$ are the estimated of $\sigma(t)$ and $g(t)$, respectively. The constants $\chi_0, \chi_1 > 0$ should be chosen sufficiently large in the reverse order. The observer's state variables are satisfying in finite time the inequalities

$$\begin{cases} |z_0-\sigma(t)| \le \mu_0\varepsilon \\ |z_1-g(t)| \le \mu_1\varepsilon^{\frac{1}{2}} \end{cases} \tag{8}$$

where μ_0, μ_1 are positive constants depending exclusively on the choose of parameters. When exact measurement for σ, $\varepsilon = 0$, any solution of the observation error satisfies the following differential inclusion (Referred to proof in Appendix B of (Shtessel et al, 2007)):

$$\begin{cases} \dot{\sigma}_0 = -\chi_0 L^{\frac{1}{2}}|\sigma_0|^{\frac{1}{2}}\mathrm{sign}(\sigma_0)+\sigma_1 \\ \dot{\sigma}_1 \in -\chi_1 L\mathrm{sign}(\sigma_1-\dot{\sigma}_0)+[-L, L] \end{cases}$$

with $\sigma_0 = z_0 - \sigma(t)$, $\sigma_1 = z_1 - g(t)$, z_0 and z_1 are observations of $\sigma(t)$ and $g(t)$, respectively. Consequently, there is $z_0{=}\sigma(t), z_1{=}g(t)$ in a finite time.

Note 1 (finite-time stability (Shtessel et al, 2007)). If a system is asymptotically stable at the origin with a finite settling time for any solution and initial conditions, it is finite-time stable at the origin.

Note 2 (Filippov differential inclusion (Levant, 2005)). A differential inclusion $\dot{x}\in F(x)$ is called a Filippov differential inclusion if the vector set $F(x)$ is non-empty, closed, convex, locally bounded and upper-semicontinuous. It is said that a differential equation $\dot{x} = f(x)$ with a locally-bounded Lebesgue-measurable right-hand side is understood in the Filippov sense, if it is replaced by a special Filippov differential inclusion $\dot{x}\in F(x)$.

From Lemma 1, it can be concluded that when $\omega(t)$ in (4) is exactly measurable, the observation errors ε_1 and ε_2 of (6) can convergence within finite time, thus, $\widehat{d}_1 = d_1$ after finite-time transient process of the observer (5).

Remark 1. Choosing appropriate observer parameters λ_1 and λ_2 can accurately estimate the term d_1 within a finite time. The larger the parameters are selected, the better the convergence of the observer will be. However,if the parameters are selected too large, it will cause the tracking overshoot, and the control input u will exceed the actual physical limit.

Remark 2. This paper introduces the FDO to estimate the disturbance term, and the precise estimation and compensation of disturbance estimation reduce the influence of disturbance on the control. It enhances the robustness of the controlled system and alleviates the chattering problem in the SMC. Nevertheless, it should be pointed out that the chattering problem is not solved.

3.2 NFTSM-FDO design

This subsection proposes the NFTSM surface and the fast sliding mode control law. The finite-time trajectory tracking controller is designed based on the FDO and the SMC theory to improve the fast-response performance.

Considering fast convergence, chattering suppression, and singularity problems, we construct the NFTSM switching function as follows:

$$s = e + \mu_1\dot{e}^{\alpha_1}\mathrm{sign}(\dot{e}) + \mu_2 e^{\alpha_2}\mathrm{sign}(e) \tag{9}$$

where $e{=}\varphi{-}\varphi_{ref}$ is the yaw angle tracking error. $\mu_1{>}0$, $\mu_2 > 0$, $\alpha_2 > \alpha_1$, $1 < \alpha_1 = q/p < 2$, p and q are both odd numbers.

The differential of s can be calculated as follows:

$$\begin{aligned} \dot{s} &= \dot{e} + \mu_1\alpha_1|\dot{e}|^{\alpha_1-1}\ddot{e} + \mu_2\alpha_2|e|^{\alpha_2-1}\dot{e} \\ &= \dot{e} + \mu_1\alpha_1|\dot{e}|^{\alpha_1-1}(\ddot{\varphi}-\ddot{\varphi}_{ref}) + \mu_2\alpha_2|e|^{\alpha_2-1}\dot{e} \\ &= \dot{e}+\mu_2\alpha_2|e|^{\alpha_2-1}\dot{e}+\mu_1\alpha_1|\dot{e}|^{\alpha_1-1}\Bigg(\frac{(C_{r0}L_r-C_{f0}L_f)\beta}{I_{z0}} \\ &\quad -\frac{C_{r0}L_r^2+C_{f0}L_f^2}{I_{z0}v_x}\omega+\frac{C_{f0}L_f}{I_{z0}}u-\ddot{\varphi}_{ref}+d_1\Bigg) \end{aligned} \tag{10}$$

When $\dot{s} = 0$, the system states reach the sliding mode surface,and the dynamics of the system occurs according to the following nonlinear differential equation:

$$\dot{e} + \mu_2\alpha_2|e|^{\alpha_2-1}\dot{e} + \mu_1\alpha_1|\dot{e}|^{\alpha_1-1}\Bigg(\frac{(C_{r0}L_r - C_{f0}L_f)\beta}{I_{z0}} - \frac{C_{r0}L_r^2 + C_{f0}L_f^2}{I_{z0}v_x}\omega + \frac{C_{f0}L_f}{I_{z0}}u - \ddot{\varphi}_{ref} + d_1\Bigg) = 0 \quad (11)$$

To avoid chattering and improve the rapid convergence of the controlled system, combining with the condition that the system states reach the sliding mode surface, i.e., $s\dot{s}<0$, the reaching law is given as follows (Yu et al, 2005):

$$\dot{s} = -k_1 s - k_2|s|^{\alpha_3}\mathrm{sign}(s) \quad (12)$$

where $0<\alpha_3<1$. k_1, k_2 are adjustable positive constants.

Remark 3. The parameters k_1, k_2 are selected as positive constants to ensure the system's stability. Meanwhile, when system states are far from the sliding mode surface, the system states will move towards the sliding mode surface with a larger gain. When the states are close to the sliding mode surface, the system states will approach the sliding mode surface with a slight gain to weaken the chattering amplitude of the controlled system. Accordingly, the fixed constants in the controller cannot be too small and cannot be too large.

When the system states approach the sliding mode surface, they are still affected by parameter perturbations and external disturbances. Therefore, the following NFTSMC law based on the FDO is designed to ensure the robustness of the whole reaching process:

$$u = \frac{I_{z0}}{L_f C_{f0}}\Bigg(\ddot{\varphi}_{ref} - \widehat{d}_1 - \frac{\beta}{I_{z0}}(L_r C_{r0} - L_f C_{f0}) + \frac{C_{r0}L_r^2 + C_{f0}L_f^2}{I_{z0}v_x}\omega - \frac{|\dot{e}|^{2-\alpha_1}\mathrm{sign}(\dot{e})}{\mu_1\alpha_1}\mu_2\alpha_2|e|^{\alpha_2-1} - \frac{|\dot{e}|^{2-\alpha_1}\mathrm{sign}(\dot{e})}{\mu_1\alpha_1} - k_1 s - k_2|s|^{\alpha_3}\mathrm{sign}(s)\Bigg) \quad (13)$$

3.3 Stability analysis of the closed-loop control system

For the controlled system (4) with the FDO (5), if the NFTSM controller is designed by (13) with the sliding mode surface (9), then the closed-loop control system is stable, and the yaw angle tracking error converges to zero in finite time. Specifically, the analysis is given as follows.

The Lyapunov function is constructed as $V = \frac{1}{2}s^2$. Calculating the time derivative of V is as follows.

$$\begin{aligned}\dot{V} &= s(\dot{e} + \mu_1\alpha_1|\dot{e}|^{\alpha_1-1}\ddot{e} + \mu_2\alpha_2|e|^{\alpha_2-1}\dot{e}) \\ &= s\mu_2\alpha_2|e|^{\alpha_2-1}\dot{e} + s\Bigg(\dot{e} + \mu_1\alpha_1|\dot{e}|^{\alpha_1-1}\Bigg(\frac{(C_{r0}L_r - C_{f0}L_f)\beta}{I_{z0}} - \frac{C_{r0}L_r^2 + C_{f0}L_f^2}{I_{z0}v_x}\omega + \frac{C_{f0}L_f}{I_{z0}}u - \ddot{\varphi}_{ref} + d_1\Bigg)\Bigg)\end{aligned} \quad (14)$$

Substituting the NFTSMC law (13) into (14) and considering the FDO's accurate estimate for the disturbance in finite time, there is

$$\begin{aligned}\dot{V} &= -k_1\mu_1\alpha_1|\dot{e}|^{\alpha_1-1}s^2 - k_2\mu_1\alpha_1|\dot{e}|^{\alpha_1-1}|s|^{\alpha_3+1} \\ &= -2\Lambda_1 V - 2^{\frac{\alpha_3+1}{2}}\Lambda_2 V^{\frac{\alpha_3+1}{2}} \\ &\le -cV^{\alpha}\end{aligned} \quad (15)$$

where $\Lambda_1 = k_1\mu_1\alpha_1|\dot{e}|^{\alpha_1-1}$, $\Lambda_2 = k_2\mu_1\alpha_1|\dot{e}|^{\alpha_1-1}$, $c = 2^{\alpha}\Lambda_2$, $\alpha = \frac{\alpha_3+1}{2}$. k_1, k_2 and μ_1 are positive numbers. The parameters α_1 and α are satisfies with $1 < \alpha_1 < 2$ and $0 < \alpha < 1$, respectively.

According to the sufficient condition of the finite-time stability (Proposition 12 in (Moulay and Perruquetti, 2006)), if $c > 0$, $0 < \alpha < 1$ and $V \ge 0$, then $s \to 0$ in an finite time. It should be noted that $c > 0$ when $\dot{e} \ne 0$ and $c = 0$ when $\dot{e} = 0$. But as long as e is not equal to 0, its derivative $\dot{e}$ is not always 0, and then c is going to be greater than 0 again. So it always is gotten $s \to 0$. Once $s = 0$, the yaw angle tracking error of the system will converge rapidly to zero in finite time.

As a result, the design flowchart of the FDO-NFTSMC strategy is shown in Fig. 4.

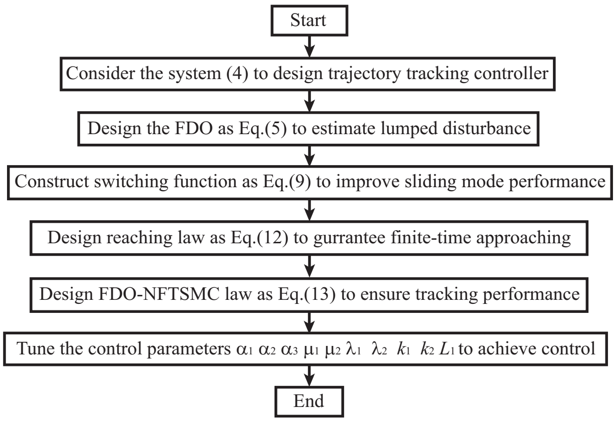

Fig. 4. FDO-NFTSMC strategy design flowchart.

4. SIMULATION VERIFICATION

4.1 Simulation environment description

The designed robust finite-time trajectory tracking control strategy is verified on the co-simulation platform of Simulink and CarSim 2016.1, shown in Fig. 5.

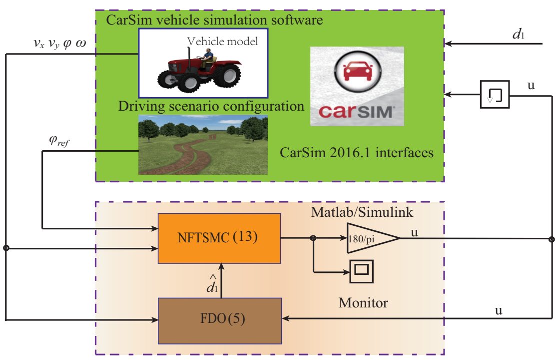

Fig. 5. Co-simulation framework of Simulink and CarSim.

In the simulation verification, the controlled plant is a complete vehicle model in CarSim with setting parameters rather than the model (4) in Fig. 3. CarSim also provides the configuration of the driving environment and trajectory of the vehicle operation. In a farming vehicle driving environment, the most common thumb-shaped trajectory is selected according to the row spacing and the shape of the actual farmland to verify the tracking performance of the designed control strategy by the linear and multi-curvature changes trajectory. The designed control strategy consisting of the FDO (5) and the NFTSMC law (13) is built-in Matlab/Simulink.

Fig. 6 shows the simulation scenario and depicts the reference trajectory of curvature and yaw angle over time. The curvature is calculated from the vehicle's turning radius R of driving, $C = 1/R$. Over time, the trajectory curve indicates whether the vehicle is in a thumb or a straight line to demonstrate the trajectory tracking performance in the straight or turning process under the controller's action.

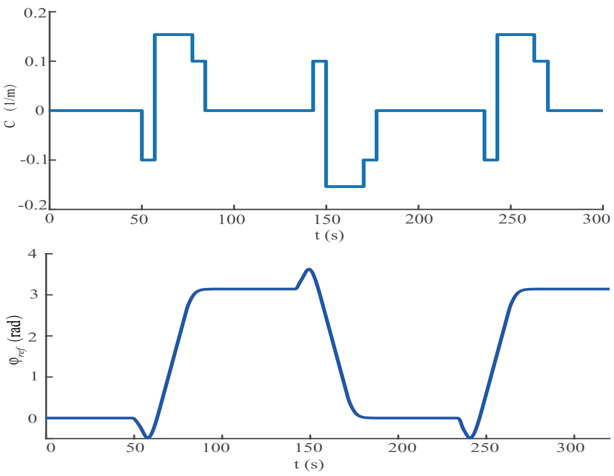

Fig. 6. Reference trajectories of curvature and yaw angle.

The relevant model parameters of a farming vehicle are shown in Table 2.

Table 2. Vehicle model parameters.

Variables	m	I_z	l_f	l_r	C_f	C_r
Unit	kg	kg.m^2	m	m	N/rad	N/rad
Value	3000	1765	1.05	1.00	96475	106475

In the simulation, the controller parameters are chosen as

$$\alpha_1 = 25/17, \quad \alpha_2 = 1.55, \quad \mu_1 = 9, \quad \mu_2 = 24.5,$$
$$\alpha_3 = 0.98, \quad k_1 = 85, \quad k_2 = 86.$$

and the FDO parameters are chosen as

$$\lambda_1 = 8.775, \quad \lambda_2 = 142.5, \quad L_1 = 10$$

Remark 4. It is important to note that the control parameters should be carefully selected in the light of practical implementation, as tracking performance is often affected by limited control energy, physical and structural constraints, and measurement noise. Therefore, information such as convergence speed, tracking error, and physical constraints is weighed during parameter adjusting. The selection criteria of the control parameters are as follows. The values of α_1, α_2, and α_3 should consider the compromise between the convergence speed and the chattering suppression. The larger the value is, the faster the convergence speed will be, but the more serious the chattering will be. Similarly, the parameters μ_1, μ_2, k_1, and k_2 should be adjusted by considering the convergence speed, tracking error, and chattering suppression. As for FDO's parameter tuning criteria, some of the instructions in Remark 1 may be helpful. Of course, all parameters set a rough range following these criteria, and specific determination can only be adjusted according to repeated empirical trials.

4.2 The comparative strategies

In order to clearly show the effectiveness and advantage of the designed NFTSM-FDO controller, we select two existing control strategies for comparison, the traditional ADRC strategy in (Lin et al, 2019) and an ADRC-SMC strategy in (Wu et al, 2019). The reason for choosing these two strategies for comparison is that the extended state observer (ESO) of the ADRC is another effective estimation for the lumped disturbance, and the ADRC-SMC strategy in (Wu et al, 2019) uses the nonsingular terminal sliding mode (NTSM) and ADRC. Moreover, they both are designed for the trajectory tracking control of the ground vehicles' yaw angle.

To ensure a fair comparison, the three control strategies' simulation environment and operating conditions are consistent. Meanwhile, the control parameters of the two controllers are carefully adjusted and determined according to the design criteria given in the controller's literature.

The ADRC strategy (Lin et al, 2019) in the simulation comparison is set as:

$$u_{adrc} = k_1 e_1 + k_2 e_2 + k_3 e_3 - z_4/b$$

where $k_1 = 42875.6$, $k_2 = 4637.4$, $k_3 = 108.3$.

The ADRC-SMC strategy (Wu et al, 2019) in the comparison is set as:

$$u_{adrc-smc} = -\left(u_0 + z_3\right)/b,$$
$$u_0 = \frac{1}{\lambda\eta}\mathrm{sign}(z_2)|z_2|^{2-\eta} + k_1 s + k_2 \tanh(s)$$

where $\lambda = 0.042$, $\eta = 19/11$, $k_1 = 650.93$, $k_2 = 386.4$.

4.3 Effectiveness and advantage verification

Firstly, consider the normal case that the road adhesion coefficient μ is a normal value of 0.6, and there is no consideration of system parameter perturbations and disturbance. Fig. 7 and Fig. 8 show the simulation results of the closed-loop control system under the NFTSM-FDO. Fig. 7 and Fig. 8 show that the tracking errors of the lateral position and yaw angle are controlled within small ranges by the designed NFTSM-FDO controller, which meets the tracking accuracy requirements. Meanwhile, the front-wheel steering angle response maintains within a reasonable physical limit.

Secondly, the comparison is given for the NFTSM-FDO, ADRC, and ADRC-SMC, considering the road adhesion coefficient $\mu = 0.3$. Fig. 9 shows the position X-Y and the yaw angle tracking responses. Fig. 10 is the yaw angle and lateral offset tracking errors. Fig. 11 shows the control input and the estimate of the disturbance (slippy) by the FDO. The NFTSM-FDO controller can quickly

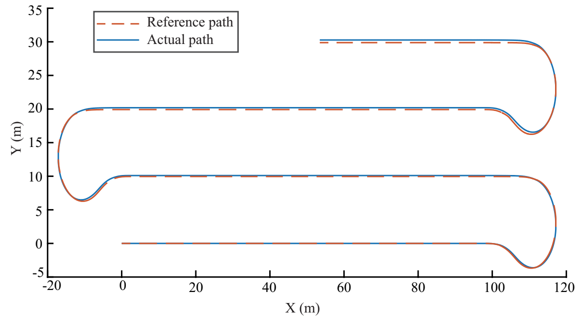

(a) Position tracking response.

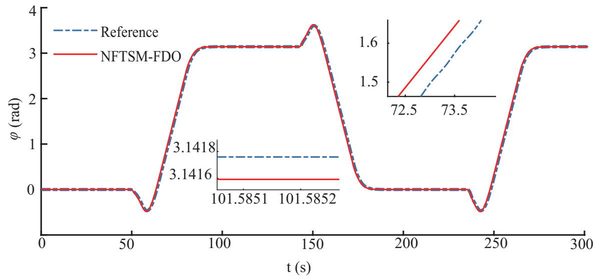

(b) Yaw angle tracking response.

Fig. 7. Trajectory tracking responses.

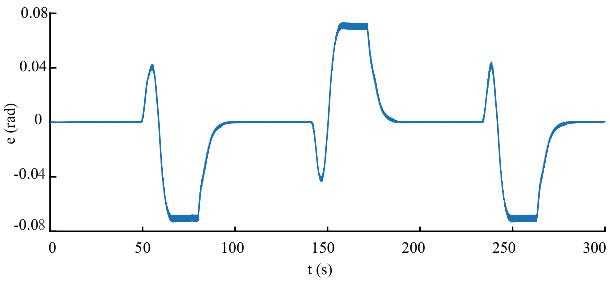

(a) Yaw angle tracking error.

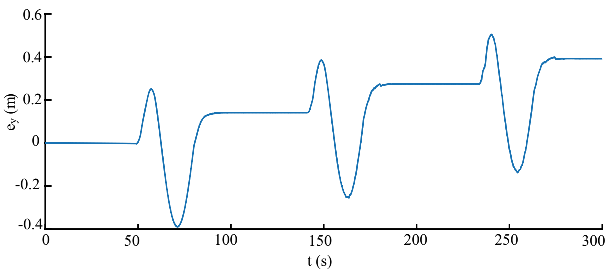

(b) Lateral direction tracking error.

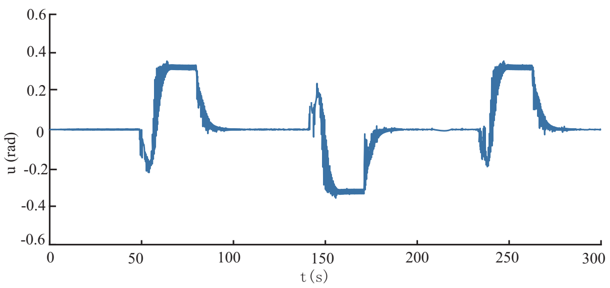

(c) Front wheel steering angle.

Fig. 8. Tracking errors and control input.

respond to environmental changes and disturbances and promptly change the vehicle's yaw angle to track the reference signal. At the same time, the observer can estimate the disturbance and compensate for the influence of the disturbance on track. ADRC-SMC is slightly inferior to NFTSM-FDO in terms of fast convergence disturbance suppression and tracking error, ensuring the controller's tracking performance. ADRC can also compensate for the influence of disturbance on the system, but the fast-tracking characteristics are not as good as the other two controllers. The proposed NFTSM-FDO controller has small steady-state tracking accuracy and fast-tracking response features. However, the average dynamic error in the steering process is greater than that of the ADRC. Fig.11 (b) shows the estimation effect of FDO on the system state and disturbance, which means that FDO can accurately and quickly estimate the system state and disturbance in the driving process.

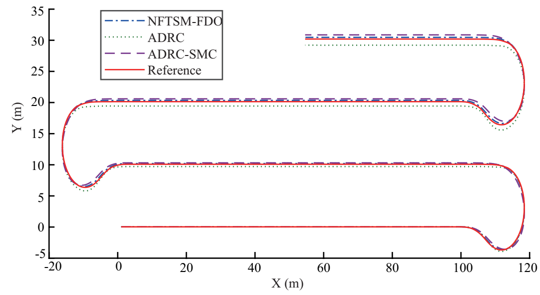

(a) Position tracking responses.

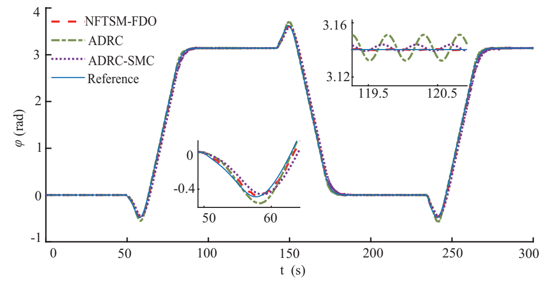

(b) Yaw angle tracking responses.

Fig. 9. Trajectory tracking responses with road slippery.

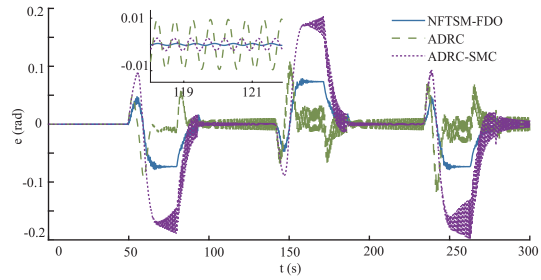

(a) Yaw angle tracking errors.

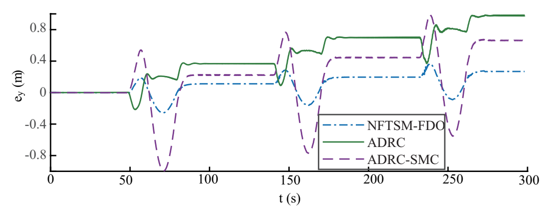

(b) Lateral direction tracking errors.

Fig. 10. Tracking errors considering road slippery.

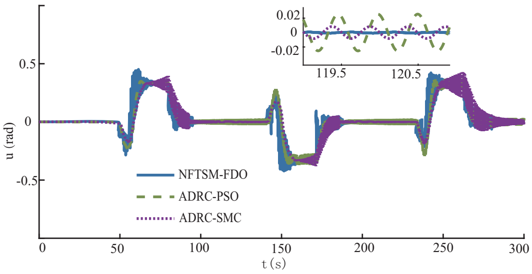

(a) Front wheel steering angle.

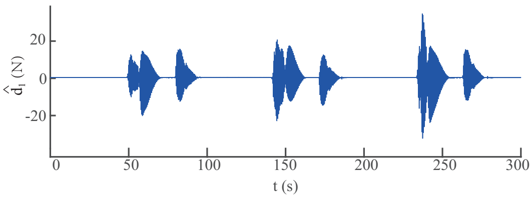

(b) Estimate of the disturbance by the FDO.

Fig. 11. Control input and FDO considering road slippery.

Furthermore, 30% system parameter perturbation and the slippy (road adhesion coefficient as 0.3) are considered. Fig. 12 shows the position X-Y and yaw angle tracking responses under the three control strategies. Fig. 13 is the yaw angle and lateral offset tracking errors. Fig. 14 shows the control input and the estimate of the disturbance (slippy) by the FDO.

From Fig. 12, when the system is disturbed, NFTSM-FDO control performance is better than the ADRC control strategy for transient system effect, and the adjustment time under NFTSM-FDO is much shorter than ADRC control performance. In addition, the NFTSM-FDO controller has high tracking accuracy in the process of line path tracking, the version of ADRC-SMC is slightly higher than that of the latter, but the capability of disturbance suppression is more robust than that of the latter.

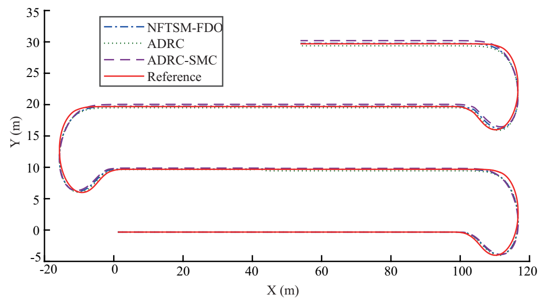

(a) Position tracking responses.

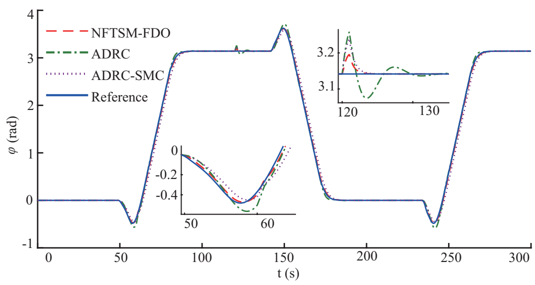

(b) Yaw angle tracking responses.

Fig. 12. Trajectory tracking with parameter perturbations.

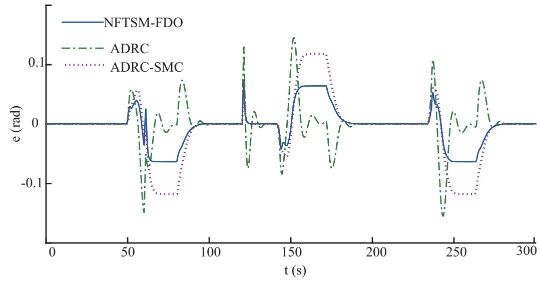

(a) Yaw angle tracking errors.

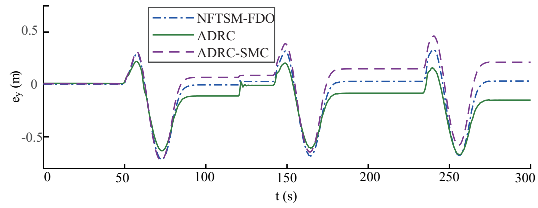

(b) Lateral direction tracking errors.

Fig. 13. Tracking errors with parameter perturbations.

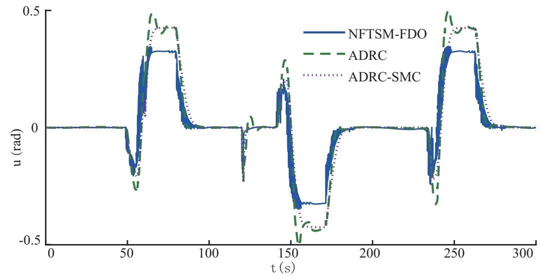

(a) Front wheel steering angle.

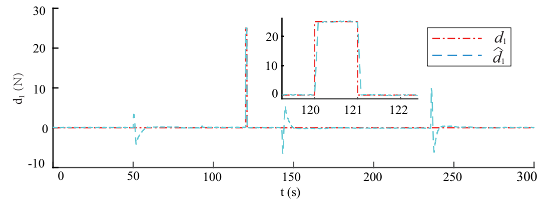

(b) Estimate of the disturbance by the FDO.

Fig. 14. Control input and FDO.

As can be seen from the simulation figures, the three controllers all complete the tracking task with high precision in straight-line tracking. Under the respective control of NFTSM-FDO and ADRC-SMC, the corresponding closed-loop control system can quickly adapt to the trajectory's dynamic change than the ADRC and make dynamic adjustments continuously with a specific tracking error. According to Fig. 13, the tracking error during the dynamic adjustments of NFTSM-FDO is smaller than that under the action of the ADRC-SMC controller. The response speed of the ADRC strategy is slower than that of the other two controllers, but it can realize the turning process with lower dynamic error than the other two controllers.

When the system is disturbed at $t = 120s$, FDO can accurately estimate the disturbance within $0.1s$, enhancing the system's robustness and improving the tracking accuracy. The results show that compared with the other two strategies, the NFTSM-FDO controller can ensure quick tracking performance and maintain low tracking errors during the whole tracking process.

5. CONCLUSION

This paper discussed the NFTSM-FDO control strategy to enhance the system performances of self-driving farming vehicles with wheel slip disturbances and parameter uncertainties. The controller has good robust tracking performance for the nonlinear and uncertain system and can achieve convergence of the finite-time tracking error due to its fast characteristics. The FDO is used for real-time estimation of the internal uncertainty of the system and the disturbance of the external environment, making the disturbance processing ability more rapid and robust. Vehicle simulation software set different operating and environmental conditions, and the control method's fast, good tracking performance and robustness were verified.

In future work, the control of the longitudinal speed of the farming vehicle will be considered cooperatively to enhance the control performance. In addition, the control algorithm will be further investigated to improve the smoothness of trajectory tracking.

REFERENCES

Bochtis, D. D., SRensen, C. G., and Busato, P. (2014). Advances in agricultural machinery management: a review, *Biosystems Engineering*, 126:69–81.

Chao, C., Gao, H., Ding, L., Li, W., Yu, H., and Deng, Z. (2018). Trajectory tracking control of wmrs with lateral and longitudinal slippage based on active disturbance rejection control, *Robotics and Autonomous Systems*, 107:32–43.

Cui, R., Chen, L., Yang, C., and Chen, M. (2017). Extended state observer-based integral sliding mode control for an underwater robot with unknown disturbances and uncertain nonlinearities, *IEEE Transactions on Industrial Electronics*, 64(8):6785–6795.

Geng, C., Mostefai, L., and Dena, M. (2009). Direct yaw-moment control of an inwheel-motored electric vehicle based on body slip angle fuzzy observer, *IEEE Transactions on Industrial Electronics*, 56(5):1411–1419.

Jiang, Y., Ding, S., Zhao, D., and Ji, W. (2015). Straight-line tracking control of an agricultural vehicle with finite-time control technique, *Asian Journal of Control*, 17(6):2218–2228.

Jiao, X., Zhang, J., and Shen, T. (2014). An adaptive servo control strategy for automotive electronic throttle and experimental validation, *IEEE Transactions on Industrial Electronics*, 61(11):6275–6284.

Levant, A. (2005). Homogeneity approach to high-order sliding mode design, *Automatica*, 41(5):823–830.

Li, S., Wu, C., and Sun, Z. (2016). Design and implementation of clutch control for automotive transmissions using terminal-sliding-mode control and uncertainty observer, *IEEE Transactions on Vehicular Technology*, 65(4): 1890–1898.

Li, S., Xu, H., Ji, Y., Cao, R., Zhang, M., and Li, H. (2019). Development of a following agricultural machinery automatic navigation systems, *Computers and Electronics in Agriculture*, 158:335–344.

Lin, Z., Jiao, X., and Wang, Z. (2019). ADRC-based active front steering strategy for path tracking of a farm vehicle, *2019 3rd Conference on Vehicle Control and Intelligence (CVCI)*.

Lipinski, A. J., Markowski, P., Lipinski, S., and Pyra, P. (2016). Precision of tractor operations with soil cultivation implements using manual and automatic steering modes, *Biosystems Engineering*, 145:22–28.

Lv, S., and Wang, N. (2017). Nonsingular terminal sliding mode based trajectory tracking control of an autonomous surface vehicle with finite-time convergence, *International Symposium on Neural Networks*, 83–92.

Matveev, A. S., Hoy, M., Katupitiya, J., and Savkin, A. V. (2013). Nonlinear sliding mode control of an unmanned agricultural tractor in the presence of sliding and control saturation, *IET Power Electronics*, 61(9):973–987.

Moulay, E., and Perruquetti, W. (2006). Finite time stability and stabilization of a class of continuous systems, *Journal of Mathematical Analysis and Applications*, 323(2):1430–1443.

Piyabongkarn, D., Grogg, J. A., and Lew, J. Y. (2009). Development and experimental evaluation of a slip angle estimator for vehicle stability control, *IEEE Transactions on Control Systems Technology*, 17(1):78–88.

Roshanianfard, A., Noguchi, N., Okamoto, H., and Ishii, K. (2020). A review of autonomous agricultural vehicles, *The experience of Hokkaido University Journal of Terramechanics*, 91:155–183.

Shtessel, Y. B., Shkolnikov, I. A., and Levant, A. (2007). Smooth second-order sliding modes: missile guidance application, *Automatica*, 43(8):1470–1476.

Soudbakhsh, D., and Eskandarian, A. (2011). Comparison of linear and non-linear controllers for active steering of vehicles in evasive maneuvers, *Proceedings of the Institution of Mechanical Engineers*, 226(2):215–232.

Sun, Z., Zheng, J., Man, Z., Fu, M., and Lu, R. (2019). Nested adaptive super-twisting sliding mode control design for a vehicle steer-by-wire system, *Mechanical Systems & Signal Processing*, 122:658–672.

Tzounis, A., Katsoulas, N., Bartzanas, T., and Kittas, C. (2017). Internet of things in agriculture, recent advances and future challenges, *Biosystems Engineering*, 164:31–48.

Watanabe, M., and Sakai, K. (2021). Novel power hop model for an agricultural tractor with coupling bouncing, stick-slip, and free-play dynamics, *Biosystems Engineering*, 204:156–169.

Wang, W., and Li, S. (2012). Finite-time trajectory tracking control of underactuated autonomous surface vessels based on non-singular terminal sliding mode, *Australian Journal of Electrical and Electronics Engineering*, 9(3): 235–246.

Wu, Y., Wang, L., Zhang, J., and Li, F. (2019). Path following control of autonomous ground vehicle based on nonsingular terminal sliding mode and active disturbance rejection control, *IEEE Transactions on Vehicular Technology*, 68(7):6379-6390.

Xia, Y., Pu, F., Li, S., and Gao, Y. (2016). Lateral path tracking control of autonomous land vehicle based on ADRC and differential flatness, *IEEE Transactions on Industrial Electronics*, 63(5):3091-3099.

Yu, S., Yu, X., Shirinzadeh, B., and Man, Z. (2005). Continuous finite-time control for robotic manipulators with terminal sliding mode, *Automatica*, 41(11):1957–1964.